HHS Public Access

Author manuscript

Proc SPIE Int Soc Opt Eng. Author manuscript; available in PMC 2015 May 27.

Published in final edited form as:

Proc SPIE Int Soc Opt Eng. 2010 January 23; 7551: . doi:10.1117/12.843184.

Spectroscopic evaluation of photodynamic therapy of the intraperitoneal cavity

Jarod C. Finlay[a], **Julia L. Sandell**[a], **Timothy C. Zhu**[a], **Robert Lewis**[b], **Keith A. Cengel**[a], and **Stephen M. Hahn**[a]

[a]Department of Radiation Oncology, University of Pennsylvania, Philadelphia, PA USA 19104

[b]Department of Surgery, University of Pennsylvania, Philadelphia, PA USA 19104

Abstract

We present the results of spectroscopic measurements of diffuse reflectance and fluorescence before and after photodynamic therapy of healthy canine peritoneal cavity. Animals were treated intra-operatively after iv injection of the benzoporphyrin derivative (BPD). The small bowel was treated using a uniform light field projected by a microlenstipped fiber. The cavity was then filled with scattering medium and the remaining organs were treated using a moving diffuser. Diffuse reflectance and fluorescence measurements were made using a multi-fiber optical probe positioned on the surface of various tissues within the cavity before and after illumination. The measured data were analyzed to quantify hemoglobin concentration and oxygenation and sensitizer concentration.

Keywords

photodynamic therapy; Benzoporphyrin; diffuse reflectance; fluorescence

1. INTRODUCTION

Photodynamic therapy (PDT) is a cancer treatment which utilizes a photosensitizing drug activated by exposure to light to excite oxygen to its singlet state. Our group and others have previously investigated the use of PDT for intraoperative applications, particularly in the thoracic [1–3] and peritoneal [4–8]cavities. When working in areas of the body, such as the intraperitoneal cavity, that are inaccessible before surgery, it is particularly challenging to perform dosimetric measurements. The question of light dosimetry during Photofrin-mediated PDT has been investigated previously.[9]

While much work has been done characterizing the in-vivo properties of tissues, this characterization is dependent on wavelength, treatment conditions, and sensitizer, so experience with one sensitizer does not necessarily translate to another. This manuscript reports preliminary results of a pre-clinical study of intraperitoneal PDT using Benzoporhyrin derivative (BPD, Visudyne, QLT, Inc). in a series of healthy canines.

Reflectance and fluorescence measurements are made intra-operatively during surgery, allowing *in-vivo* assessment of tissue oxygenation, hemoglobin concentration, and sensitizer concentration.

2. METHODS

2.1 Animal Preparation and treatment

A total of 15 healthy dogs were used in this study. Each dog was sensitized with 0.25 mg/Kg BPD (one animal at 0.125 mg/Kg), followed by a 3–6 hour drug-light interval. Animals were then anesthetized and underwent partial bowel resection to simulate the effects of an invasive tumor debulking procedure. The treatment proceeded in two steps. First, the bowel was treated in sections sequentially using a circular light field produced byt an overhead optical fiber tipped with a microlens. The illumination was provided by a 689-nm diode laser (B&W Tek, Inc.). The fluence rate on the surface was monitored continuously using isotropic fiber-optic based light detectors. Second, the bowel was shielded and the cavity was filled with a light-scattering solution of intralipid and illuminated with a 689 nm light at 10 or 2 J/cm^2 *via* a light diffusing probe. Light dose was monitored at 7 points throughout the cavity to ensure uniform dose.

2.2 Reflectance and Fluorescence Measurements

Diffuse reflectance and fluorescence measurements were made before and after PDT treatment. One of two optical probes was used to measure the reflectance. Both of these probes use 365-micron core optical fibers to deliver white light (for reflectance measurements) or 403-nm light (for fluorescence measurements), and identical fibers for the collection of the remitted light. The first-generation probe consisted of one source fiber and 10 detection fibers. The second generation probe, shown in figure 1, is of similar design, but uses two adjacent source fibers, one for white light and a second for 403-nm excitation. The source fibers were couples to a tungsten lamp (Avalight, Avantes, Inc.), and a 403-nm diode laser (Power Technology, Inc.), respectively. The detector fibers were coupled into a CCD-based spectrograph (InSpectrum, Roper Scientific). The illumination of the probe was switched by electronically controlled shutters, one built into the white light source, and a second fiber-coupled source for the 403-nm source. A multichannel, USB-coupled, digital input/output (I/O) board was used to synchronize the switching of the shutters and the acquisition of spectra by the CCD. This I/O board also controlled a multi-color light-emitting diode (LED) indicator on the handle of the probe and sampled the position of the adjacent pushbutton. The reflectance and fluorescence spectra were measured by placing the probe in contact with the organ tissue (organs measured are: abdominal wall, aorta, bladder, bowel, gall bladder, kidney, liver, stomach, and skin) by the surgeon. When the CCD was ready to acquire data, the indicator LED was illuminated. When the surgeon was satisfied with the position of the probe, he pressed the pushbuttion on the handle, which triggered the sequential acquisition of reflectance, background, and fluorescence spectra. The sequence was repeated 6 times for each site, and the resulting spectra were averaged to reduce noise. The background-subtracted reflectance spectra were corrected for the spectral variation of the lamp and sensitivity of the CCD by dividing by the spectrum measured with the same instrument in an integrating sphere with spectrally uniform reflectance.

The reflectance was measured by placing the probe in contact with the organ tissue (organs measured are: abdominal wall, aorta, bladder, bowel, gall bladder, kidney, liver, stomach, and skin) by the surgeon. With several detection fibers making up the probe, a separate spectrum was recorded for each fiber. The resulting data were corrected for the CCD offset by subtracting spectra that was taken with the shutter closed. Ambient light corrections were made by subtracting the white collected from the sample surface with no light illuminating the source fiber. This subtraction is sample specific was performed uniquely for each sample. There is wavelength dependence in the source intensity and spectrograph sensitivity which is accounted for by dividing each spectrum by the measured reflectance of an integrating sphere. The integrating sphere is wavelength-independent and has Lambertian reflectance. The reflectance measurements taken for each dog ranged from 5–8 organs, each organ measured pre and post illumination. The wavelength calibration of the spectrograph was checked and correct when necessary. This correction was based on a measurement of the spectrum of the overhead fluorescent lights (which were covered by filters during surgery) made on the day of the measurements.

2.3 Reflectance Analysis

A graphical user interfaced (GUI) based program was developed in Matlab to process data from the spectrograph. Data is read into a program called *Process_spe* and is put into a Matlab matrix. In this program, data can be corrected for noise, offset, lamp spectrum, and divided by the integrating sphere spectrum as sescribed above. The user is allowed to specify the optical probe used, the calibration wavelength, and detector noise. Once the data has been processed, the user can display the spectrum so as to view any erroneous data, identifying it as a poor candidate for further analysis. Each step in the data processing is interactive.

A second GUI was developed in Matlab to fit the processed data. *Spectrextract* reads the processed data (now in Matlab matrix format) and allows the user to interactively fit the spectra. One can specify the range of wavelengths to be considered, the source-detector distances considered, the model, algorithm, and fit parameters. The option is offered to fit data as a function of wavelength, source-detector separation, or both simultaneously. This interactive process aids the user to find the optimal fit for each spectrum (see Fig. 2)

2.4 Single separation fitting

Spectrextract allows for a wide variety of possible combinations of fitting algorithms and parameters; new models can be added and modified and parameters can be adjusted uniquely or set at default values. In this study the data was fit using a reflectance model developed by Finlay and Foster which uses Matlab's built-in function *fminsearch* to fit the data. The Finlay-Foster model uses a hybrid diffusion-P3 approximation [10] which models light propagation in a turbid medium. The absorption spectrum is assumed to be a linear combination of the known spectra of absorbers present in the tissue. In this instance, the absorption spectra of deoxy- and oxy-hemoglobin are combined with a Gaussian representing the absorption due to BPD The parameters of this Guassian were determined from *in vivo* absorption spectra obtained in a murine model (data not shown) . . The reduced scattering spectrum was assumed to be of the form $\mu_s' = A\,(\lambda/\lambda_0)^{-b}$ In addition to the other

user-defined parameters, the range of wavelengths considered can be set, typically taken at 550–700 nm so that we observe spectra where water does not dominate. The fitting program outputs free parameters of the oxyand deoxy- hemoglobin concentrations, and scattering spectrum. Each spectrum was fitted independently in this at multiple source-detector separations.

2.5 Fluorescence data analysis

In order to correct the measured fluorescence spectra for the effects of tissue optical properties, we divided the fluorescence spectrum by the reflectance spectrum measured at the same source-detector separation. Similar corrections have been reported previously.[11–13] This correction is approximate, but, as shown in figure 3, is effective in reducing the effects of hemoglobin absorption on the fluorescence spectrum, and on equalizing the amplitudes of fluorescence measured at different source-detector separations.

To quantify the fluorescence of BPD, we performed a singular value decomposition (SVD) fitting algorithm to fit the data with a linear combination of two basis spectra. The first is a background spectrum acquired from the abdominal wall of one animal, with the region of emission of BPD (670 To 735 nm) interpolated to eliminate the effect of BPD. The second is the emission of BPD from the same animal, with the background subtracted. An exponentially-weighted Fourier series is also included in the fit to account for the presence of unknown fluorophores, as described previously. [13], The result of the fit is an amplitude of each component, which is proportional to the concentration of the sensitizer and the combination of chemical species that contribute to the background, respectively.

3. RESULTS

3.1 Reflectance

We applied the data processing and analysis procedure to the data taken from 15 healthy dogs administered BPD. We compiled the data according to post or pre illumination, organ, and date. Averages were taken of the oxyhemoglobin, deoxyhemoglobin, and total hemoglobin concentration and the hemoglobin oxygen saturation (StO_2). With respect to the reflectance measurements we noticed no particular trend or relationship between individual dogs or organs when comparing pre and post treatment. While the characteristic double absorption peak of oxyhemoglobin is still clearly visible there did not appear to a characteristic change in spectra between pre and post treatment data. The variations observed between samples are larger than what PDT can typically induce and point to heterogeneities between individual dogs. We expect the heterogeneity because of the nature of tissue and the non-uniform distribution of blood vessels, which changes the optical properties of a sample in a non-uniform. Table 1 presents the mean results we compiled for the reflectance measurements of this study.

3.2 Fluorescence

The fluorescence emission of each animal was quantified. Because the bowel was the one of the only organs in which an interpretable fluorescence signal was obtained in all 15 animals , we present here the results for the fluorescence measured in the bowel. The value

of the BPD fluorescence is plotted two ways: First, in terms of the raw amplitude. This amplitude is corrected for optical properties by dividing by the reflectance spectrum at the same source-detector separation, but may still show some sensitivity to source intensity variations and geometrical effects not accounted for by this correction. This amplitude is shown in figure 4.

The same data, normalized by dividing by the background amplitude, is also shown. This normalization allows a direct evaluation of the ratio of BPD fluorescence to autofluorescence, which is independent of instrumentation artifacts and indicates the relative concentrations of BPD and the components (collagen, NADH, elastin, etc) which contribute to autofluorescence. In both cases, the values measured before and after PDT illumination are shown. No systematic changes in BPD fluorescence are evident.

4. DISCUSSION

We have presented reflectance and fluorescence data obtained *in vivo* from canines undergoing intraperitoneal BPD-mediated PDT. While these data are preliminary and the analysis is ongoing, they allow us to make draw several conclusions. First, the heterogeneity in optical properties, hemoglobin concentration, and tissue oxygenation is significant both among animals and among different organs and locations in a single animal. A similar pattern has been observed in spectroscopic data collect *in vivo* from the human patients undergoing a clinical trial for prostate PDT.[14] This observation motivates the further development of dosimetry systems for PDT that make use of patient-specific and even location-specific optical data and dosimetric monitoring to optimize light does. It is unlikely that dosimetry performed with a single set of optical properties and sensitizer concentrations will be sufficient for an arbitrary patient. Work in this area is ongoing in our group and several others.

Second, we do not observe systematic changes in hemodynamics as a result of PDT treatment, despite the fact that a physiological response to the treatment has been observed in many of the animals. This indicates that the treatment regimen we employ has not induced either drastic vascular shutdown leading to induced hypoxia or consistent changes in blood volume. Previous studies have shown, however, that the vascular response to PDT can be remarkably complicated [15] and may depend quite sensitively on the details of the drug pharmacokinetics. [16] It is therefore difficult to draw detailed conclusions regarding the vascular and cellular response to PDT at any given location.

Third, we do not observe systematic changes in BPD fluorescence resulting from PDT. It is possible that this is an indication that the spatial , intra-animal, and inter-animal variation obscures any small systematic changes. Even in this case, our results provide evidence that BPD photobleaching *in vivo* is not as severe as that observed for other sensitizers, such as ALA-induced PpIX [13,17,18] and Photofrin [19]. A typical treatment using these sensitizers would reduce the sensitizer emission to a small fraction of its initial value.

ACKNOWLEDGEMENTS

The authors which to thank Andreea Dimofte for assistance with dosimetry, and QLT, Inc. for providing BPD. Funding for this work was provided in part by NIH grants P01 CA87971 and R01 CA109456.

REFERENCES

1. Finlay JC, Zhu TC, Dimofte A, Friedberg JS, Hahn SM. Diffuse reflectance spectra measured in vivo in human tissues during Photofrin-mediated pleural photodynamic therapy. Proc. SPIE. 2006; 6139:61390O.
2. Friedberg JS, Mick R, Stevenson JP, Zhu TC, Busch TM, Shin D, Smith D, Culligan M, Dimofte A, Glatstein E, Hahn SM. Phase II Trial of Pleural Photodynamic Therapy and Surgery for Patients With Non-Small-Cell Lung Cancer With Pleural Spread. J. Clin. Onc. 2004; 22(11):2192–2201.
3. Pass HI, Tochner Z, DeLaney T, Smith P, Friauf W, Glatstein E, Travis W. Intraoperative photodynamic therapy for malignant mesothelioma. Ann Thorac Surg. 1990; 50(4):687–688. [PubMed: 2222072]
4. Cengel KA, Glatstein E, Hahn SM. Intraperitoneal photodynamic therapy. Cancer treatment and research. 2007; 134:493–514. [PubMed: 17633077]
5. Hendren SK, Hahn SM, Spitz FR, Bauer TW, Rubin SC, Zhu T, Glatstein E, Fraker DL. Phase II trial of debulking surgery and photodynamic therapy for disseminated intraperitoneal tumors. Annals of surgical oncology. 2001; 8(1):65–71. [PubMed: 11206227]
6. Hahn SM, Fraker DL, Mick R, Metz J, Busch TM, Smith D, Zhu T, Rodriguez C, Dimofte A, Spitz F, Putt M, Rubin SC, Menon C, Wang HW, Shin D, Yodh A, Glatstein E. A phase II trial of intraperitoneal photodynamic therapy for patients with peritoneal carcinomatosis and sarcomatosis. Clin Cancer Res. 2006; 12(8):2517–2525. [PubMed: 16638861]
7. Griffin GM, Zhu T, Solonenko M, Del Piero F, Kapakin A, Busch TM, Yodh A, Polin G, Bauer T, Fraker D, Hahn SM. Preclinical evaluation of motexafin lutetium-mediated intraperitoneal photodynamic therapy in a canine model. Clin Cancer Res. 2001; 7(2):374–381. [PubMed: 11234893]
8. Bauer TW, Hahn SM, Spitz FR, Kachur A, Glatstein E, Fraker DL. Preliminary report of photodynamic therapy for intraperitoneal sarcomatosis. Annals of surgical oncology. 2001; 8(3): 254–259. [PubMed: 11314943]
9. Vulcan TG, Zhu TC, Rodriguez CE, Hsi A, Fraker DL, Baas P, Murrer LH, Star WM, Glatstein E, Yodh AG, Hahn SM. Comparison between isotropic and nonisotropic dosimetry systems during intraperitoneal photodynamic therapy. Lasers in surgery and medicine. 2000; 26(3):292–301. [PubMed: 10738292]
10. Hull EL, Foster TH. Steady-state reflectance spectroscopy in the P3 approximation. JOSA A. 2001; 18:584–599.
11. Muller MG, Georgakoudi I, Zhang Q, Wu J, Feld MS. Intrinsic fluorescence spectroscopy in turbid media: Disentangling effects of scattering and absorption. Appl. Opt. 2001; 40:4633–4646. [PubMed: 18360504]
12. Wu J, Feld MS, Rava RP. Analytical model for extracting intrinsic fluorescence in turbid media. Appl. Opt. 1993; 32:3583–3595.
13. Finlay JC, Conover DL, Hull EL, Foster TH. Porphyrin bleaching and PDT-induced spectral changes are irradiance dependent in ALA-sensitized normal rat skin in vivo. Photochem. Photobiol. 2001; 73:54–63. [PubMed: 11202366]
14. Finlay JC, Zhu TC, Dimofte A, Stripp D, Malkowicz SB, Busch TM, Hahn SM. Interstitial fluorescence spectroscopy in the human prostate during motexafin lutetium-mediated photodynamic therapy. Photochem Photobiol. 2006; 82:1270–1278. [PubMed: 16808592]
15. Busch TM. Local physiological changes during photodynamic therapy. Lasers in surgery and medicine. 2006; 38(5):494–499. [PubMed: 16788920]
16. Chen B, Pogue BW, Hoopes PJ, Hasan T. Vascular and cellular targeting for photodynamic therapy. Critical reviews in eukaryotic gene expression. 2006; 16(4):279–305. [PubMed: 17206921]

17. Robinson DJ, de Bruijn HS, van der Veen N, Stringer MR, Brown SB, Star WM. Fluorescence photobleaching of ALA-induced protoporphyrin IX during photodynamic therapy of normal hairless mouse skin: The effect of light dose and irradiance and the resulting biological effect. Photochem. Photobiol. 1998; 67:140–149. [PubMed: 9477772]

18. Robinson DJ, de Bruijn HS, van der Veen N, Stringer MR, Brown SB, Star WM. Protoporphyrin IX fluorescence photobleaching during ALA-mediated photodynamic therapy of UVB-induced tumors in hairless mouse skin. Photochem. Photobiol. 1999; 69:61–70. [PubMed: 10063801]

19. Finlay JC, Mitra S, Foster TH. Photobleaching kinetics of Photofrin in vivo and in multicell tumor spheroids indicate multiple simultaneous bleaching mechanisms. Phys. Med. Biol. 2004; 49:4837–4860. [PubMed: 15584523]

Figure 1.
end-view of the optical probe used for reflectance and fluorescence measurements, and operator's-eye view showing the operator control.

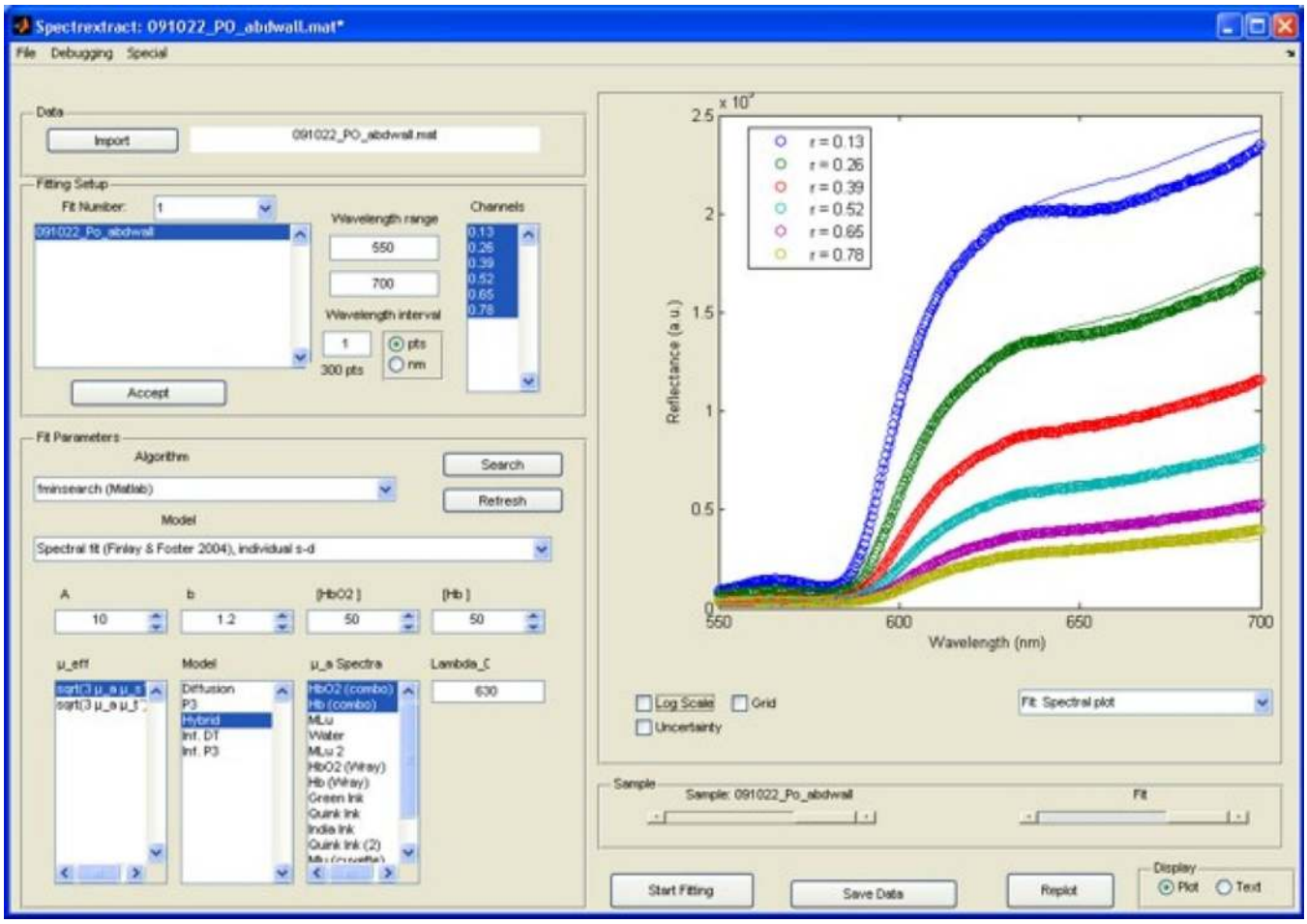

Figure 2.

Modular fitting platform, including an ‘Algorithim’ list and ‘Model’ list, displaying a fit for the spectra of a post-PDT abdominal wall.

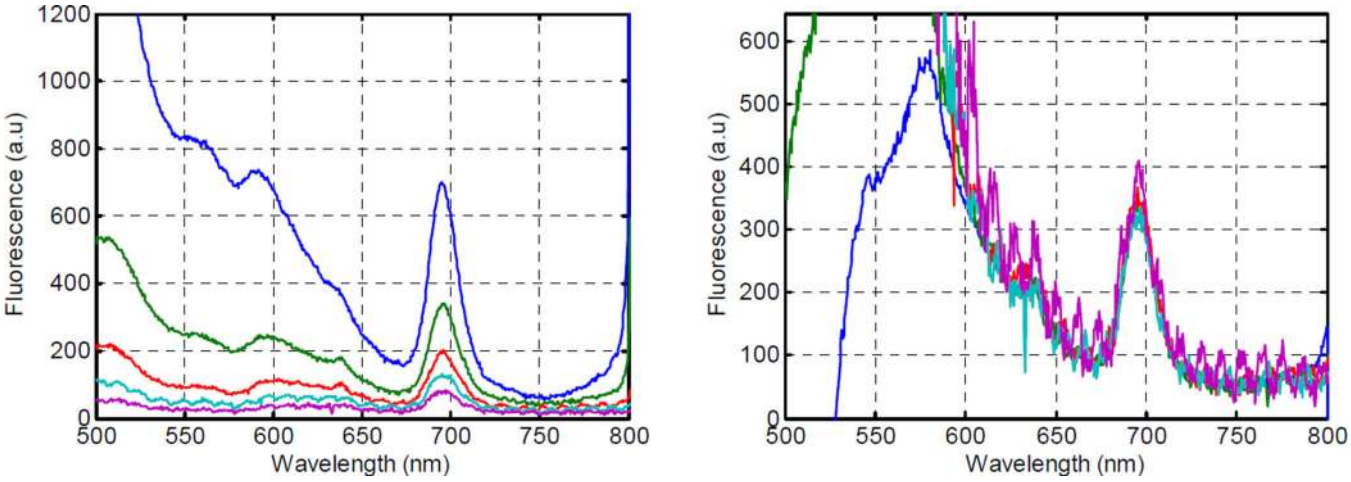

Figure 3.

Typical fluorescence emission spectrum obtained *in vivo* (left) and the same sample after correction by division by reflectance at the same source-detector separation (right).

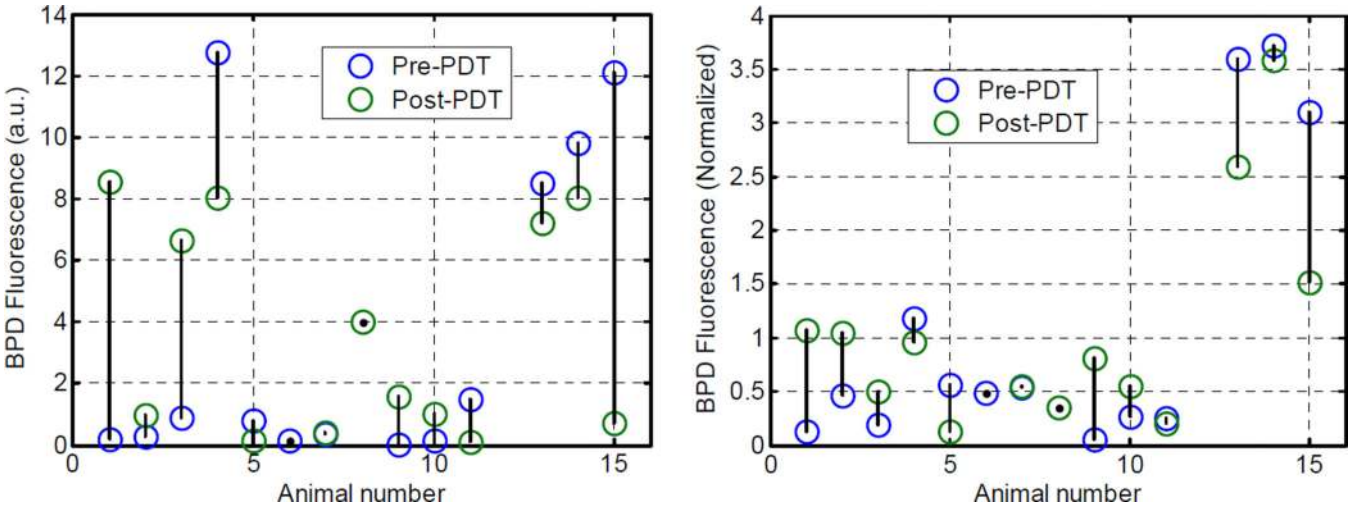

Figure 4.

Fluorescence emission from BPD observed in the canine bowel (left). The amplitude divided by the background amplitude is also shown (right).

Table 1

Mean values of total hemoglobin and StO_2 for canine organs undergoing BPD PDT

Organ	N dog	N Samples		Total Hemoglobin (uM)		STO2(%)	
				Pre PDT	Post PDT	Pre PDT	Post PDT
Abdominal Wall	15	8	Mean	188.0	149.07	61.32	58.41
			Std	289.91	214.71	40.36	34.94
Aorta	15	7	Mean	64.88	240.62	64.88	69.08
			Std	44.09	294.97	44.09	19.32
Bowel	15	5	Mean	144.78	93.69	55.03	47.62
			Std	80.67	47.33	28.30	27.34
Kidney	15	4	Mean	117.13	269.09	120.94	309.81
			Std	22.28	352.02	19.96	369.82
Liver	15	3	Mean	115.29	118.47	3.77	118.47
			Std	61.24	27.28	6.54	27.28
Stomach	15	8	Mean	64.95	145.27	64.95	369.83
			Std	37.14	214.79	37.14	888.26

Proc SPIE Int Soc Opt Eng. Author manuscript; available in PMC 2015 May 27.